

Process analysis of nuclear hydrogen production via intermediate temperature SOEC electrolysis

Authors: Guan, Chengzhi, Shao, Qing, Lu, Yue, Jin, Dun, Luo, Linghong, Wang, Xiulin, Yao, Huichao, Dai, Ruoyun, Xiao, Guoping, Wang, Jianqiang, Guan, Chengzhi, Luo, Linghong, Xiao, Guoping, Wang, Jianqiang

Date: 2025-09-28T00:00:00+00:00

Abstract

When the operating temperature of a Solid Oxide Electrolysis Cell (SOEC) is lower than the outlet temperature of a nuclear reactor, the reactor can be directly coupled with the SOEC as a high-temperature heat source. However, the key to the efficiency and return on investment of this hybrid energy system lies in the expected lifetime of the SOEC. This study assessed Ni-YSZ|YSZ|GDC|LSC fuel electrode support cells' long-term stability during electrolysis at 650 oC with a current density of $-0.5 \text{ A} \cdot \text{cm}^{-2}$ over 1818 h. The average voltage degradation rate of $2.63\% \cdot \text{kh}^{-1}$ unfolded in two phases: an initial rapid decay (90 to 1120 h at $3.58\% \cdot \text{kh}^{-1}$) and a stable decay (1120 to 1818 h at $2.14\% \cdot \text{kh}^{-1}$), emphasizing SOECs' probability coupling with nuclear reactors at 650 oC. Post-1818-hour electrolysis revealed nickel particle formation associated with $\text{Ni}(\text{OH})_x$ diffusion and re-deposition, alongside a strontium-containing layer causing interface cracking. Despite minimal strontium segregation in the EDS, XPS data indicated surface segregation of Sr. This study provides crucial insights into prolonged SOEC operation, highlighting both its potential and challenges.

Full Text

Preamble

Process Analysis of Nuclear Hydrogen Production via Intermediate Temperature SOEC Electrolysis

Qing Shao^{1,2,†}, Yue Lu^{2,†}, Dun Jin², Ling-Hong Luo^{1,‡}, Xiu-Lin Wang³, Hui-Chao Yao³, Ruo-Yun Dai³, Cheng-Zhi Guan^{2,4,5,§}, Guo-Ping Xiao^{2,4,¶}, and Jian-Qiang Wang^{2,4,5,**}

¹School of Materials Science and Engineering, Jingdezhen Ceramic University, Jingdezhen 333403, China

²Department of Hydrogen Technique, Shanghai Institute of Applied Physics, Chinese Academy of Sciences, Shanghai 201800, China

³CNOOC Gas and Power Group/R&D Center, Beijing 100020, China

⁴Key Laboratory of Interfacial Physics and Technology, Chinese Academy of Sciences, Shanghai 201800, China

⁵Shanghai Hyenergy Technology Co., Ltd., Shanghai 201800, China

When the operating temperature of a Solid Oxide Electrolysis Cell (SOEC) is lower than the outlet temperature of a nuclear reactor, the reactor can be directly coupled with the SOEC as a high-temperature heat source. However, the key to the efficiency and return on investment of this hybrid energy system lies in the expected lifetime of the SOEC. This study assessed the long-term stability of Ni-YSZ|YSZ|GDC|LSC fuel electrode support cells during electrolysis at 650 °C with a current density of $-0.5 \text{ A} \cdot \text{cm}^{-2}$ over 1818 h. The average voltage degradation rate of $2.63\% \cdot \text{kh}^{-1}$ unfolded in two phases: an initial rapid decay (90 to 1120 h at $3.58\% \cdot \text{kh}^{-1}$) and a stable decay (1120 to 1818 h at $2.14\% \cdot \text{kh}^{-1}$), emphasizing the feasibility of coupling SOECs with nuclear reactors at 650 °C. Post-1818-hour electrolysis revealed nickel particle formation associated with Ni(OH) diffusion and re-deposition, alongside a strontium-containing layer causing interface cracking. Despite minimal strontium segregation in the EDS, XPS data indicated surface segregation of Sr. This study provides crucial insights into prolonged SOEC operation, highlighting both its potential and challenges.

Keywords: Nuclear hydrogen production, SOEC, Stability, Intermediate temperature

Introduction

The rising global demand for energy, coupled with ambitious decarbonization targets, has catalyzed a significant shift towards more sustainable energy systems. As traditional energy sources increasingly fall out of favor owing to their environmental impacts, the spotlight has turned to alternatives that promise not only reduced carbon footprints but also robust reliability and scalability [1,2]. Among these, nuclear power is particularly promising. Unlike many renewable energy sources, which are often intermittent, such as solar and wind energy, nuclear power offers a steady and reliable flow of energy [3,4]. Moreover, it does so without the direct emission of greenhouse gases, which are a major contributor to climate change [5]. The role of nuclear energy extends beyond simply providing electricity; it is increasingly regarded as a versatile player in the energy sector, capable of supporting various industrial processes through the generation of combined heat and power [6]. This multipurpose utility is crucial in the broader context of creating more integrated and efficient energy systems. One of the most significant aspects of nuclear energy's potential is its ability to produce hydrogen [7].

Hydrogen is increasingly viewed as a critical element for transitioning to a sus-

tainable energy future. It serves as a clean energy carrier, an effective solution for energy storage, and a valuable feedstock for numerous industrial processes [8-10]. Producing hydrogen through nuclear power not only satisfies the energy system's need for low-carbon solutions but also aligns with global efforts to establish a more sustainable, reliable, and diversified energy supply chain [11]. To harness this potential effectively, advanced nuclear reactor technologies, such as Very High-Temperature Reactors (VHTR), Supercritical Water Reactors (SCWR), and Molten Salt Reactors (MSR), have been developed. These reactors are designed to provide the high-temperature heat necessary for efficient large-scale industrial applications, including hydrogen production [12]. The VHTR is notable for its use of helium as a coolant, which allows it to reach temperatures exceeding 1000 °C. Such high temperatures make VHTRs ideal for thermochemical hydrogen production, a process that can split water into hydrogen and oxygen at high efficiencies [13,14]. Meanwhile, intermediate-temperature reactors, which operate at lower temperatures than VHTRs, can still play a pivotal role in hydrogen production through technologies such as Solid Oxide Electrolysis Cells (SOEC) [7,15].

SOECs represent a compelling technology for hydrogen production, capable of leveraging both electrical and thermal energy from nuclear reactors. These cells operate more efficiently at higher temperatures, which enhances their reaction kinetics, making them a promising option for sustainable hydrogen production [16]. In recognition of their potential, the European Union has funded numerous projects under the Fuel Cells and Hydrogen Joint Undertaking (FCH-JU) to advance SOEC technology and integrate it with existing energy systems [17,18]. Research on SOECs and their integration with nuclear power has been ongoing for several years. In 2003, the Idaho National Laboratory initiated a significant project to explore hybrid nuclear energy systems incorporating SOECs [19,20]. Various studies have examined system efficiencies under different operational conditions. For instance, Peters et al. [21] examined SOEC system efficiencies when integrated with external heat sources, finding that efficiencies could vary from 90% to 104% depending on configuration and operation. Similarly, Milewski et al. [22] explored the integration of protonic and ionic SOECs with nuclear reactors, calculating hydrogen production energy consumption at 38.83 and 37.55 kWh · kg⁻¹ respectively, which they found to be significantly efficient. Further studies, such as those by Fütterer et al. [23] within the European GEMINI+ project, examined the coupling of high-temperature gas-cooled reactor (HTGR) power plants with SOECs, suggesting that extending SOEC service life could significantly enhance hybrid system feasibility and efficiency. Yalamati et al. [24] posited that SOEC efficiency depends on the nuclear heat source used, suggesting that utilizing both electricity and waste heat from nuclear power plants could elevate hydrogen production efficiency to as much as 60%. Moreover, Zhang et al. [25] calculated thermo-hydrogen conversion efficiency for different coupling methods, finding that when all heat for SOECs is provided by a nuclear reactor, the highest efficiency is achieved with the reactor's outlet temperature at 900 °C.

Most research has focused on anode-supported and electrolyte-supported SOECs operating above 750 °C, whereas the outlet temperature of MSR is below 700 °C [26]. Considering that direct coupling offers significant advantages for large-scale hydrogen production, the outlet steam temperature of the nuclear reactor should exceed the operating temperature of the SOEC [25]. In this situation, acting as a high-temperature heat source, nuclear waste heat can be used for heating the SOEC module, gas preheating, and water vaporization [4]. To align with MSR outlet temperature, the SOEC working temperature should be lowered to a medium temperature range, approximately 650 °C.

Although high-temperature SOEC operation (>800 °C) is advantageous, it introduces challenges [27]. One primary issue at these temperatures is mutual diffusion of cell components. High temperatures can cause materials to intermingle at the molecular level, potentially degrading structural integrity over time and resulting in efficiency loss and shorter operational lifespan. Additionally, particle aggregation is a significant concern, as particles within cell materials can clump together, affecting performance by altering crucial material properties. Another challenge is sealant selection. Sealants play a critical role in maintaining SOEC integrity by ensuring components remain adequately sealed without leakage. At high temperatures, finding materials that can withstand heat while maintaining robust seals is difficult, as many common sealants degrade or lose sealing properties, posing substantial challenges to system effectiveness and safety. In response to these challenges, focus has shifted toward developing intermediate-temperature SOECs (IT-SOECs) operating at approximately 650 °C. IT-SOECs offer a promising alternative that significantly mitigates high-temperature issues, as lower temperatures impose reduced demands on connectors and seals, aligning with the trend toward mid- to low-temperature transformation of SOEC [28].

Considering that hybrid energy system efficiency and return on investment are constrained by short SOEC service life, investigating long-term stability at intermediate temperatures is crucial. This study aims to reveal alterations in electrochemical behavior through stability tests on commercial Ni-YSZ|YSZ|GDC|LSC planar cells, specifically targeting electrolysis at 650 °C. Through voltage-over-time curves and post-testing microscopic analysis, degradation mechanisms within various cell components under intermediate temperatures were explored. Extensive R&D in this field highlights the synergy between nuclear power and hydrogen production as a beacon of hope for a more sustainable energy future. By leveraging advanced nuclear technologies and innovative hydrogen production methods such as SOECs, we can move closer to achieving a low-carbon, high-efficiency energy system that meets global demands while adhering to stringent environmental standards.

II. Experimental

A. Description of the Hybrid Energy System

The schematic depicted in Fig. 1 [Figure 1: see original paper] illustrates a nuclear-powered hydrogen production system in which the primary energy source is the MSR. In this system, coolant salt heated in the MSR core is directed into a heat exchanger, which plays a pivotal role in transferring the immense thermal energy to other parts of the system. Following heat exchange, thermal energy facilitates electricity generation via a turbine and generator setup. The electricity produced is strategically distributed to serve two purposes: a portion is fed into the electrical grid, contributing to general power supply, while the remainder is specifically allocated to power SOECs for water electrolysis, the key step in hydrogen production. Additionally, this electricity ensures smooth functioning of various system components, including pumps, separators, and compressors, which are essential for maintaining operational continuity and system integrity.

The exchanged heat is utilized for heating the SOEC module, gas preheating, and water vaporization, all essential in the hydrogen production pathway. Notably, the gas produced by the SOEC still possesses high heat value, which is subsequently released to processes such as water vaporization through another heat exchanger (simplified in the diagram). This repurposing of waste heat significantly enhances thermal efficiency. In the system shown in Fig. 1, heating of the SOEC module, water vaporization, and gas superheating are powered by waste heat from the MSR. Within this framework, only the electricity required for SOEC water electrolysis (P_{SOEC}) and the power needed to run other components such as pumps and compressors (P_{comp}) are supplied by MSR-generated electricity. This design effectively utilizes MSR thermal energy for process heating, optimizing energy efficiency by repurposing waste heat for critical thermal processes while relying on MSR-generated electricity for operations that require it. This integrated approach enhances overall energy efficiency and sustainability, with corresponding efficiency calculated as Eq. (1) [25]:

$$\eta = (m \cdot \text{HHV}) / (P_{SOEC} + P_{comp})$$

where m is the mass flow rate of produced hydrogen, and HHV is the high-heat value of hydrogen ($\text{HHV} = 285.8 \text{ kJ} \cdot \text{mol}^{-1}$). The HHV includes energy released from both hydrogen combustion to form water and subsequent condensation of water vapor into liquid water.

B. Cell and Test System Description

This study examined commercial fuel electrode-supported cells, with detailed preparation documented in preceding articles [16]. As presented in Fig. 2 [Figure 2: see original paper], cell cross-sectional microstructure was explored using scanning electron microscopy (SEM), providing comprehensive understanding of material interfaces and layer continuity essential for optimizing performance.

At the bottom is a fuel electrode support layer comprising approximately 400 μm of Ni/3YSZ (yttria-stabilized zirconia). This substantial thickness ensures mechanical robustness, allowing the cell to withstand stresses encountered during elevated-temperature operation and dynamic electrolysis conditions. This support layer is complemented by an active fuel electrode layer featuring Ni/8YSZ composition with approximately 12 μm thickness. A thinner active layer is tailored for enhanced catalytic activity and increased ionic conductivity, crucial for the electrolysis process. Further analysis reveals a 3 μm electrolyte layer; this very thin electrolyte is critical for maintaining high ionic conductivity while ensuring minimal electronic leakage. The thinness substantially reduces ohmic losses, ensuring attainment of high current densities at the relatively lower operational temperature of 650 $^{\circ}\text{C}$. This is followed by a 3 μm gadolinium-doped ceria (GDC) barrier layer, which plays an integral role in mitigating chemical reactivity and inter-diffusion issues between the YSZ electrolyte and $\text{La}_{0.6}\text{Sr}_{0.4}\text{CoO}_3$ δ (LSC) oxygen electrode. GDC was chosen for its excellent ionic conductivity and chemical compatibility with both YSZ and LSC. This layer aids in stabilizing the triple-phase boundary (TPB) where electrochemical reactions occur, thus enhancing overall efficiency and longevity. Additionally, the cell comprises a 12 μm LSC (lanthanum strontium cobaltite) oxygen electrode, noteworthy for its compatibility with intermediate-temperature operations compared to other oxygen electrode materials. The cell dimensions were 5 cm \times 5 cm, with the air electrode measuring 4 cm \times 4 cm, providing an active area of 16 cm^2 for meaningful industrial application scenarios.

C. Experimental Procedure

Experimental assessments involved current-voltage polarization curves to explore initial cell performance. The fuel electrode was supplied with 80% steam content while operating temperature was varied between 600, 650, 700, and 750 $^{\circ}\text{C}$ to investigate temperature impact on SOEC performance. Stability testing over prolonged periods is crucial for understanding operational viability. Subsequently, a current density of $-0.5 \text{ A} \cdot \text{cm}^{-2}$ was applied at 650 $^{\circ}\text{C}$ to explore stability. Steam content was maintained at 80%, as this partial pressure was considered to increase cell voltage and gas diffusion impedance [29,30].

To gain insights into degradation mechanisms, post-test characterization was performed using scanning electron microscopy (SEM, Carl Zeiss, Germany) and energy dispersive spectrometry (EDS, Zeiss Merlin Compact, Germany) to analyze the microstructure and composition of the “aging cell” subjected to 1800 h of stability testing. SEM analysis provided detailed insights into morphological changes during long-term operation, while EDS analysis revealed compositional shifts such as depletion of active elements and formation of secondary phases that could negatively affect electrochemical performance. A reference electrolysis cell from the same production batch, subjected only to reduction, served as a comparison point that maintained original microstructural and compositional integrity during cycling. Comparing the aging cell with this reference specimen

allowed clearer understanding of degradation processes, highlighting the extent of degradation in the aged cell.

To align with molten salt nuclear reactor outlet temperature, which is below 700 °C [26], SOEC operating temperature was reduced to approximately 650 °C. Consequently, the electrolysis cell was placed in a furnace set to 650 °C to simulate SOEC-MSR coupling. Electrochemical performance was evaluated using a custom-designed integrated testing station. As shown in Fig. 3 [Figure 3: see original paper], this setup provided a highly controlled environment essential for reproducible and precise measurements. The gas supply system manages feed gases for both electrodes (typically hydrogen, steam, and air) using high-quality mass flow controllers essential for maintaining desired compositions and ratios. For the fuel electrode, gas composition was 80% steam and 20% hydrogen, with flow rates of 230 ml · min⁻¹ for steam and 58 ml · min⁻¹ for hydrogen, the latter serving as protective gas to prevent Ni oxidation. On the oxygen electrode side, pure air was supplied at 1152 ml · min⁻¹. The testing station's core capability includes various electrochemical tests such as Electrochemical Impedance Spectroscopy (EIS), current-voltage (I-V) measurements, and durability testing, all instrumental for evaluating performance under different conditions. Accurate temperature control via a thermal management system is indispensable, and this testing system design ensures reliability and reproducibility of the electrolysis process, as detailed in previous studies [16].

III. Results and Discussion

Initial Performance and Evolution of the Cell

Initial experiments conducted through current-voltage (I-V) polarization tests, depicted in Fig. 4a [Figure 4: see original paper], provided crucial data on SOEC electrochemical behavior under operational conditions. These tests establish a baseline for assessing durability and long-term stability. The I-V polarization curves were tested under a steam flow rate of 230 ml · min⁻¹ at the fuel electrode and 1152 ml · min⁻¹ of air at the air electrode. Cell performance varied across 600–750 °C, demonstrating an inverse relationship between temperature and open circuit voltage, coherent with Nernst equation predictions [31]:

$$E = E^0 - (RT/2F) \ln(\text{PH}_2 \cdot \text{PO}_2^{0.5} / \text{PH}_2\text{O})$$

Here, E^0 represents the theoretical voltage in the standard state (Nernst electromotive force), R is the gas constant, T is absolute temperature, F is Faraday's constant, and the number of electrons transferred is 2. PH_2O and PH_2 represent partial pressures of steam and hydrogen in the fuel electrode, respectively, while PO_2 represents oxygen partial pressure in the air electrode.

At higher temperatures of 750 °C and 700 °C, the I-V curves showed current limitations where voltage increased disproportionately relative to current density, indicating non-linear characteristics. This behavior, specifically turning points at 48.48% steam conversion, likely results from concentration polariza-

tion caused by gas diffusion limitations [31]. At these higher operational temperatures, kinetic processes may be enhanced, but physical transport of reactants to the three-phase boundary (TPB) becomes limiting. Although the electrolysis cell could attain higher current density and hydrogen production efficiency at elevated temperatures, this study selected 650 °C to align with nuclear reactor outlet temperature range. At 650 °C, the I-V curve showed a linear relationship, suggesting adequate gas supply for efficient electrolysis.

Figure 4b shows Electrochemical Impedance Spectroscopy (EIS) results at different temperatures, providing critical insights into temperature effects on cell efficiency. The data demonstrate that lower temperatures increase both Ohmic and polarization impedances within the electrolysis cell, attributed to pronounced temperature effects on oxygen ion transport kinetics within the electrolyte, catalytic effectiveness of nickel (Ni), and charge transfer dynamics at the TPB [32,33]. Temperature significantly influences oxygen ion mobility in the electrolyte; lower temperatures slow kinetics, leading to higher impedance as ionic conductivity decreases. Furthermore, nickel, commonly used as fuel electrode material in SOECs, exhibits decreased catalytic activity at lower temperatures, impairing overall electrochemical reaction efficiency, particularly the hydrogen evolution reaction. The TPB, where electrolyte, electrode, and gas phase meet, is crucial for effective charge transfer. At lower temperatures, charge transfer dynamics are hindered, contributing to increased polarization impedance. Specific values such as Ohmic impedance of 0.22 Ω and polarization impedance of 0.14 Ω at 650 °C highlight more favorable conditions compared to 600 °C, where a significantly increased impedance arc is noted for the charge transfer reaction at the fuel electrode. This suggests 650 °C may be more suitable for long-term stability research, providing better conductivity and catalytic activity within the temperature window for SOEC-MSR coupling while minimizing impedance-related losses and enhancing overall performance.

The long-term stability of Solid Oxide Electrolysis Cells (SOECs) is crucial for practical application, particularly in coupling with nuclear energy systems for hydrogen production. Figure 5 [Figure 5: see original paper] presents the voltage-time (V-T) curve of the SOEC operating in galvanostatic mode, offering insights into performance and degradation behavior over an extended period. The stability test was conducted at -8 A (-0.5 A \cdot cm $^{-2}$) and 650 °C with the same atmosphere as the initial performance test. The electrolysis cell demonstrated stable operation in SOEC mode for more than 1800 h. The V-T curve can be divided into three distinct phases, each characterized by different degradation rates. During the initial 90 h, curve fitting yielded a slope of approximately -3.604×10^{-5} , indicating a degradation rate of $-3.42\% \cdot$ kh $^{-1}$. The negative slope suggests a decrease in degradation, indicating an activation process where cell components stabilize and improve performance [33]. In the following phase (90-1120 h), cell voltage increased from 1.101 V to 1.136 V, representing a linear degradation rate of approximately $3.58\% \cdot$ kh $^{-1}$. This phase is marked by rapid decay, reflecting significant degradation as reported by Wang et al. [16,34]. Throughout the steady decay period (1120-1818 h), voltage contin-

ued increasing, albeit at a slower rate. The average degradation rate during this phase was $2.14\% \cdot \text{kh}^{-1}$. The reduced slope indicates transition to a more stable degradation phase, aligning with patterns reported in Ref. [35] characterized by slower, more consistent degradation. Consequently, the long-term stability exhibited by the SOEC suggests substantial potential for coupling with nuclear energy systems for water electrolysis applications. The relatively low degradation rates, especially during the steady decay phase, indicate that SOECs can maintain efficiency over extended periods, making them suitable for continuous hydrogen production.

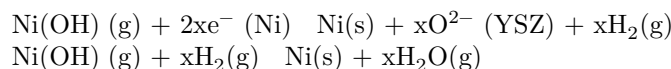
Post-Test Analysis of Cells

In studies of intermediate-temperature SOEC operation, understanding factors contributing to cell degradation is critical. SEM and EDS were employed to analyze microstructure and elemental distribution of tested cells, enabling comprehensive examination of physical and chemical changes in the fuel electrode over time. Figure 6 [Figure 6: see original paper] presents cross-sectional SEM images depicting SOEC morphology before and after stability testing. In contrast to the blocky Ni-YSZ structure shown in Fig. 6a, significant microstructural changes were observed after long-term testing (Fig. 6b). Within the Ni-YSZ functional layer of the post-testing fuel electrode, numerous particles approximately 100 nm in diameter were observed near the electrolyte interface. These particles indicate significant microstructural alterations that could impact overall performance and stability [36,37]. Additionally, SEM images highlighted microcracks and voids between the electrolyte layer and GDC barrier. These defects can impede ionic conductivity and exacerbate degradation processes, leading to further efficiency decline [38]. Furthermore, a dense layer found between the electrolyte and GDC barrier may indicate secondary phase formation, possibly resulting from interactions between electrode materials and electrolyte. These phases could contribute to degradation by introducing additional resistive interfaces within the cell, impacting overall electrochemical performance [39].

Further analysis of the Ni-YSZ fuel electrode after long-term stability testing is shown in Fig. 7 [Figure 7: see original paper]. SEM and EDS results showed no obvious Ni migration during this process. Ni migration within SOECs is a multifaceted phenomenon influenced by several factors including electrolysis current density, electric field strength and distribution caused by Ni distribution, concentration gradients of hydrogen and steam, and temperature gradients [40]. This complex process lacks definitive mechanistic explanation due to various interacting factors. The absence of pronounced Ni migration despite 1800 operational hours suggests that conditions within the cell might not have reached thresholds required for significant Ni migration, or that migration rates were too slow for detection. This finding is critical because it indicates that Ni-YSZ stability can be maintained under certain operational conditions, potentially leading to longer cell lifetimes.

EDS analysis revealed minute nickel-containing particles, as evidenced by map-

ping results shown in Fig. 8 [Figure 8: see original paper]. Mogensen et al. [41,42] attributed nickel migration dynamics to generation of Ni(OH) volatile species diffusing along vapor pressure gradients. Specifically, under elevated water vapor pressure ($P_{H_2O} > 80\%$), nickel reacts with water, resulting in higher Ni(OH) concentrations where x can be 1 or 2. In SOEC mode, current is driven by an external power source flowing from the oxygen electrode through the electrolyte to the fuel electrode, which is typically supplied with a steam-rich gas mixture. Steam is electrolyzed at the electrode into hydrogen and oxygen ions, with $x = 1$ predominant. Conversely, in SOFC mode, current is driven by fuel chemical energy flowing from fuel electrode to oxygen electrode, with pure hydrogen fuel reacting with oxide ions to release electrons and produce water as byproduct, making $x = 2$ dominant. Consequently, Ni(OH) diffuses from high to low concentration along the concentration gradient, consistent with decreasing P_{H_2O} direction. In SOFC mode, Ni(OH) diffuses from the electrolyte-fuel electrode interface toward the fuel electrode interior, while in SOEC mode, diffusion occurs from the support layer to the fuel electrode interior. This migration is driven by reactions outlined in Eqs. (3) and (4), wherein nickel is generated and subsequently deposited, contributing to Ni migration. In this investigation, an electrolysis cell was subjected to SOEC operational environment for 1818 h. Although EDS results in Fig. 7 indicate lack of significant Ni migration, observation of numerous small Ni particles within the functional layer suggests possible Ni(OH) diffusion and subsequent re-deposition.



EDS point scanning of both small-particle aggregation and block-like regions, shown in Fig. 9 [Figure 9: see original paper], provides significant insights into Ni distribution and migration. Results revealed stark contrast in Ni content between these regions, with 6.67% Ni in the blocky region and significantly higher 73.56% Ni in the particle agglomeration area. This analysis further supports previous observations, highlighting the complexity of Ni migration within SOECs and underscoring the need for further research to understand and mitigate this phenomenon. By optimizing operational parameters, conducting in-depth microstructural analyses, and exploring material innovations, SOEC stability and performance can be enhanced.

Microstructural analysis of the oxygen electrode post-electrolysis was performed using SEM and EDS, uncovering changes and potential degradation mechanisms that could significantly affect performance and durability. SEM images in Fig. 10 [Figure 10: see original paper] reveal microcracks at the oxygen electrode-electrolyte interface. These cracks undermine mechanical stability and lead to further degradation under operational stresses, accelerating cell failure [38]. Additionally, SEM images show formation of a dense layer at the interface, likely resulting from Sr segregation. EDS mapping indicates this dense layer is likely composed of strontium-containing phases such as $SrZrO_3$, an electrical insulator with poor ionic conductivity ($1.87 \times 10^{-6} \text{ S} \cdot \text{cm}^{-1}$ at 800°C) [43].

Formation of SrZrO_3 phase at the electrode/electrolyte interface can obstruct ion migration [44]. Additionally, Sr diffusion to YSZ surfaces results in Sr depletion in the LSC oxygen electrode, promoting formation of Sr-free LaCoO_3 , which has significantly reduced electrocatalytic activity for the oxygen reduction reaction (ORR) [45]. Emergence of these Sr-containing high-resistance phases, along with potential electrolyte cracking, is expected to increase overall cell resistance [46,47], leading to higher energy losses and decreased efficiency that pose significant challenges for long-term operation.

In SOEC analysis, EDS mapping indicated that Sr segregation toward the cell surface was not significant. To gain deeper understanding of surface chemistry and potential segregation phenomena, XPS was employed to examine chemical composition and environment, particularly Sr oxidation state, in both reference and aged SOECs. Results depicted in Fig. 11 [Figure 11: see original paper] show Sr 3d photoelectron spectra for both samples along with corresponding Sr elemental percentages. Figure 11a illustrates Sr 3d peak fitting for the reference cell, while Fig. 11b shows fitting outcomes for the aged sample. The Sr 3d energy level exhibited a dual state: the low binding energy state of $3d_{5/2}$ (indicative of lattice Sr) appeared at approximately 131.9 eV, while the high binding energy state of $3d_{3/2}$ (corresponding to surface Sr) was observed at approximately 133.3 eV [48]. These surface states are speculated to consist of a composite of SrO , $\text{Sr}(\text{OH})_2$, and SrCO_3 [49,50]. Quantitative analysis revealed that the proportion of surface Sr to total Sr increased from 39.42% in the reference sample to 49.5% in the aged sample, implying that despite absence of significant intensity differences in EDS mapping, there is increased tendency for Sr segregation toward the electrolysis cell surface after 1818 h of operation.

Sr segregation in LSC electrodes is a well-documented phenomenon influenced by factors such as material stoichiometry [51], strain [52], temperature [51], oxygen partial pressure [53], LSC microstructure [54], and electrochemical polarization [55]. In this study, relatively mild electrolysis conditions suggest that Sr segregation to the LSC electrode surface is likely driven by Sr reaction with atmospheric CO_2 or H_2O , forming stable compounds such as SrCO_3 and $\text{Sr}(\text{OH})_2$ that are more stable at the surface, thereby promoting Sr migration from bulk material to surface [47].

IV. Conclusion

To achieve direct coupling between an MSR and SOEC, robust SOEC stability below the nuclear reactor outlet temperature is required. Stability tests were conducted on fuel electrode support cells featuring Ni-YSZ|YSZ|GDC|LSC architecture at 650 °C, employing a current density of $-0.5 \text{ A} \cdot \text{cm}^{-2}$. Throughout the testing period from 90 h to 1818 h, an average voltage degradation rate of $2.63\% \cdot \text{kh}^{-1}$ was observed. This degradation process unfolded in distinct stages: an initial rapid decay phase from 90 to 1120 hours characterized by $3.58\% \cdot \text{kh}^{-1}$ degradation, followed by a stable decay process from 1120 to 1818 hours maintaining $2.14\% \cdot \text{kh}^{-1}$. These results indicate the viability of SOECs for direct

coupling with MSRs at intermediate temperatures, exhibiting minor voltage degradation at 650 °C and demonstrating commendable long-term stability.

Following 1818 h of electrolysis, minute nickel particles were observed within the Ni-YSZ fuel electrode, possibly associated with Ni(OH) diffusion and subsequent re-deposition. Concurrently, a compact strontium-containing layer formed at the oxygen electrode-electrolyte interface, leading to interface microcracking. Although pronounced Sr segregation to the surface was not evident in EDS analyses, XPS calculations revealed a tendency for Sr surface segregation.

To further improve cell stability and enhance hybrid energy system efficiency and economic return, efforts should focus on mitigating Ni migration in the fuel electrode and preventing Sr segregation in the oxygen electrode. Strategies may include optimizing material compositions, refining microstructural designs, and controlling operational parameters to reduce degradation mechanism impacts.

References

- [1] M.J.B. Kabeyi, O.A. Olanrewaju, Sustainable energy transition for renewable and low carbon grid electricity generation and supply. *Front. Energy Res.* 9, 743114 (2022). doi: 10.3389/fenrg.2021.743114
- [2] S. Chu, A. Majumdar, Opportunities and challenges for a sustainable energy future. *Nature.* 488, 294-303 (2012). doi: 10.1038/nature11475
- [3] K. Fernandez-Cosials, R. Vecino, C. Vazquez-Rodríguez, A flexible nuclear energy system using cryptoassets as enablers: Economic assessment. *Prog. Nucl. Energy.* 161, 104735 (2023). doi: 10.1016/j.pnucene.2023.104735
- [4] T. Cui, J. Zhu, Z. Lyu et al., Efficiency analysis and operating condition optimization of solid oxide electrolysis system coupled with different external heat sources. *Energy Convers.* 279, 116727 (2023). doi: 10.1016/j.enconman.2023.116727
- [5] L. Liu, H. Guo, L. Dai et al., The role of nuclear energy in the carbon neutrality goal. *Prog. Nucl. Energy.* 162, 104772 (2023). doi: 10.1016/j.pnucene.2023.104772
- [6] C.P. Marcel. Addressing the global energy problem: Perspectives, challenges, and potential solutions. *Nucl. Eng. Des.* 414, 112610 (2023). doi: 10.1016/j.nucengdes.2023.112610
- [7] R. Pinsky, P. Sabharwall, J. Hartvigsen et al., Comparative review of hydrogen production technologies for nuclear hybrid energy systems. *Prog. Nucl. Energy.* 123, 103317 (2020). DOI: 10.1016/j.pnucene.2020.103317
- [8] D.A. Cullen, K.C. Neyerlin, R.K. Ahluwalia et al., New roads and challenges for fuel cells in heavy-duty transportation. *Nat. Energy.* 6, 462-474 (2021). doi: 10.1038/s41560-021-00775-z
- [9] L. Van Hoecke, L. Laffineur, R. Campe et al., Challenges in the use of hydrogen for maritime applications. *Energy Environ. Sci.* 14, 815-843 (2021). doi: 10.1039/D0EE01545H
- [10] M. Chatenet, B.G. Pollet, D.R. Dekel et al., Water electrolysis: from text-

- book knowledge to the latest scientific strategies and industrial developments. *Chem. Soc. Rev.* 51, 4583–4762 (2022). doi: 10.1039/d0cs01079k
- [11] J. Nowotny, T. Hoshino, J. Dodson et al., Towards sustainable energy. Generation of hydrogen fuel using nuclear energy. *Int J Hydrogen Energ.* 41, 12812–12825 (2016). doi: 10.1016/j.ijhydene.2016.05.054
- [12] S. Şahin, H.M. Şahin, Generation-IV reactors and nuclear hydrogen production. *Int J Hydrogen Energ.* 46, 28936–28948 (2021). doi: 10.1016/j.ijhydene.2020.12.182
- [13] R. Ider, R. Allen, Nuclear heat for hydrogen production: Coupling a very high/high temperature reactor to a hydrogen production plant. *Prog. Nucl. Energy.* 51, 500–525 (2009). doi: 10.1016/j.pnucene.2008.11.001
- [14] A. Simpson, E. Veron, Assessment of the market opportunities for hydrogen derived from high temperature reactor driven processes. *Nucl. Eng. Des.* 398, 111961 (2022). doi: 10.1016/j.nucengdes.2022.111961
- [15] W.C. adaleti, E.G. de Souza, S.N.M. de Souza, The potential of hydrogen production from high and low-temperature electrolysis methods using solar and nuclear energy sources: the transition to a hydrogen economy in Brazil. *Int J Hydrogen Energ.* 47, 34727–34738 (2022). doi: 10.1016/j.ijhydene.2022.08.065
- [16] Q. Shao, D. Jin, Y. Lu et al., Performance evolution analysis of solid oxide electrolysis cells operating at high current densities. *Int J Hydrogen Energ.* 57, 709–716 (2024). doi: 10.1016/j.ijhydene.2024.01.096
- [17] K.R. Schultz, Production of hydrogen by fusion energy: A review and perspective. *Fusion Sci. Technol.* 44, 393–9 (2003). doi: 10.13182/FST03-A366
- [18] O. Posdziech, K. Schwarze, J. Brabandt, Efficient hydrogen production for industry and electricity storage via high-temperature electrolysis. *Int J Hydrogen Energ.* 44, 19089–101 (2019). doi: 10.1016/j.ijhydene.2018.05.169
- [19] J.E. O’ Brien, M.G. McKellar, E.A. Harvego et al., High-temperature electrolysis for large-scale hydrogen and syngas production from nuclear energy -summary of system simulation and economic analyses. *Int J Hydrogen Energ.* 35, 4808–4819 (2010). doi: 10.1016/j.ijhydene.2009.09.009
- [20] C.M. Stoots, J.E. O’ Brien, K.G. Condie et al., High-temperature electrolysis for large-scale hydrogen production from nuclear energy -Experimental investigations. *Int J Hydrogen Energ.* 35, 4861–4870 (2010). doi: 10.1016/j.ijhydene.2009.10.045
- [21] R. Peters, R. Deja, L. Blum et al., Influence of operating parameters on overall system efficiencies using solid oxide electrolysis technology. *Int J Hydrogen Energ.* 40, 7103–13 (2015). doi: 10.1016/j.ijhydene.2015.04.011
- [22] J. Milewski, J. Kupecki, A. Szcześniak et al., Hydrogen production in solid oxide electrolyzers coupled with nuclear reactors. *Int J Hydrogen Energ.* 46, 35765–35776 (2021). doi: 10.1016/j.ijhydene.2020.11.217
- [23] M.A. Fütterer, R. Pabarcus, S. Hübner et al., Nuclear process heat application options: Highlights from the European GEMINI+ project. *Nucl. Eng. Des.* 396, 111879 (2022). doi: 10.1016/j.nucengdes.2022.111879
- [24] H.P.S. Yalamati, R.K. Vij, R. Srivastava, in *Solar-Driven Green Hydrogen Generation and Storage*, ed. by R. Srivastava, J. Chattopadhyay, D.M.F. Santos (Elsevier, 2023), 347–362

- [25] W. Zhang, B. Yu, J. Xu, Efficiency evaluation of high-temperature steam electrolytic systems coupled with different nuclear reactors. *Int J Hydrogen Energ.* 37, 12060-12068 (2012). doi: 10.1016/j.ijhydene.2012.04.024
- [26] A. Di Ronco, A. Cammi, S. Lorenzi, Preliminary analysis and design of the heat exchangers for the Molten Salt Fast Reactor. *Nucl. Eng. Technol.* 52, 51-58 (2020). doi: 10.1016/j.net.2019.07.013
- [27] J. Mermelstein, O. Posdziech, Development and demonstration of a novel reversible SOFC system for utility and micro grid energy storage. *Fuel Cells.* 17, 562-570 (2017). doi: 10.1002/fuce.201600185
- [28] S.J. Kim, K.J. Kim, A.M. Dayaghi et al., Polarization and stability of $\text{La}_2\text{NiO}_4 \delta$ in comparison with $\text{La}_{0.6}\text{Sr}_{0.4}\text{Co}_{0.2}\text{Fe}_{0.8}\text{O}_3 \delta$ as air electrode of solid oxide electrolysis cell. *Int J Hydrogen Energ.* 41, 14498-14506 (2016). doi: 10.1016/j.ijhydene.2016.05.284
- [29] J. Liang, Y. Wang, J. Zhu et al., Investigation on the reaction mechanism of solid oxide co-electrolysis with different inlet mixtures based on the comparison of CO_2 electrolysis and H_2O electrolysis. *Energy Convers.* 277, 116621 (2023). doi: 10.1016/j.enconman.2022.116621
- [30] S.D. Kim, D.W. Seo, A.K. Dorai et al., The effect of gas compositions on the performance and durability of solid oxide electrolysis cells. *Int J Hydrogen Energ.* 38, 6569-6576 (2013). doi: 10.1016/j.ijhydene.2013.03.115
- [31] A. Mahmood, S. Bano, J.H. Yu et al., Performance evaluation of SOEC for $\text{CO}_2/\text{H}_2\text{O}$ co-electrolysis: Considering the effect of cathode thickness. *J. CO_2 Util.* 33, 114-120 (2019). doi: 10.1016/j.jcou.2019.05.014
- [32] V. Bilalis, B. Li, H.L. Frandsen et al., The effect of operating temperature on galvanostatic operation of solid oxide electrolysis cells. *ECS Trans.* 111, 429 (2023). doi: 10.1149/11106.0429ecst
- [33] Y. Yang, X. Tong, A. Hauch et al., Study of solid oxide electrolysis cells operated in potentiostatic mode: Effect of operating temperature on durability. *Chem. Eng. J.* 417, 129260 (2021). doi: 10.1016/j.cej.2021.129260
- [34] Y. Wang, Z. Lyu, M. Han et al., Initial-stage performance evolution of solid oxide fuel cells based on polarization analysis. *ECS Trans.* 103, 1261 (2021). doi: 10.1149/10301.1261ecst
- [35] T. Lehtinen, M. Noponen, Solid oxide electrolyser demonstrator development at elcogen. *ECS Trans.* 103, 1939 (2021). doi: 10.1149/10301.1939ecst
- [36] A. Hauch, S.D. Ebbesen, S.H. Jensen et al., Solid Oxide Electrolysis Cells: Microstructure and Degradation of the Ni/Yttria-Stabilized Zirconia Electrode. *J. Electrochem. Soc.* 155, B1184 (2008). doi: 10.1149/1.2967331
- [37] X. Sun, P.V. Hendriksen, M.B. Mogensen et al., Degradation in Solid Oxide Electrolysis Cells During Long Term Testing. *Fuel Cells.* 19, 740-7 (2019). doi: 10.1002/fuce.201900081
- [38] C.E. Frey, Q. Fang, D. Sebold, et al., A Detailed Post Mortem Analysis of Solid Oxide Electrolyzer Cells after Long-Term Stack Operation. *J. Electrochem. Soc.* 165, F357 (2018). doi: 10.1149/2.0961805jes
- [39] V. Subotić, S. Futamura, G.F. Harrington et al., Towards understanding of oxygen electrode processes during solid oxide electrolysis operation to improve simultaneous fuel and oxygen generation. *J. Power Sources.* 492, 229600 (2021).

doi: 10.1016/j.jpowsour.2021.229600

[40] L.A. Jolaoso, I.T. Bello, O.A. Ojelade, et al., Operational and scaling-up barriers of SOEC and mitigation strategies to boost H₂ production- a comprehensive review. *Int J Hydrogen Energ.* 48, 33017-41 (2023). doi: 10.1016/j.ijhydene.2023.05.077

[41] M.B. Mogensen, M. Chen, H.L. Frandsen et al., Ni migration in solid oxide cell electrodes: Review and revised hypothesis. *Fuel Cells.* 21, 415-29 (2021). doi: 10.1002/fuce.202100072

[42] M.B. Mogensen, A. Hauch, X. Sun et al., Relation Between Ni Particle Shape Change and Ni Migration in Ni-YSZ Electrodes -a Hypothesis. *Fuel Cells.* 17, 434-41 (2017). doi: 10.1002/fuce.201600222

[43] F. Wankmüller, J. Szász, J. Joos et al., Correlative tomography at the cathode/electrolyte interfaces of solid oxide fuel cells. *J. Power Sources.* 360, 399-408 (2017). doi: 10.1016/j.jpowsour.2017.06.008

[44] K. Develos-Bagarinao, H. Yokokawa, H. Kishimoto, et al., Elucidating the origin of oxide ion blocking effects at GDC/SrZr(Y)O₃/YSZ interfaces. *J Mater Chem A.* 5, 8733-43 (2017). doi: 10.1039/C7TA01589E

[45] R. Kiebach, W.W. Zhang, W. Zhang, et al., Stability of La_{0.6}Sr_{0.4}Co_{0.2}Fe_{0.8}O₃/Ce_{0.9}Gd_{0.1}O₂ cathodes during sintering and solid oxide fuel cell operation. *J. Power Sources.* 283, 151-61 (2015). doi: 10.1016/j.jpowsour.2015.02.064

[46] Z. Lu, S. Darvish, (La₁ Sr)₁δCo₁ Fe O₃ interface cathode inter-layer/electrolyte et al., SrZrO₃ Formation during sintering. *J. Electrochem. Soc.* 164, F3097 (2017). doi: 10.1149/2.0141710jes

[47] K. Chen, S.P. Jiang, Surface segregation in solid oxide cell oxygen electrodes: Phenomena, mitigation strategies and electrochemical properties. *Electrochem. Energy Rev.* 3, 730-765 (2020). doi: 10.1007/s41918-020-00078-z

[48] E. Mutoro, E.J. Crumlin, H. Pöpke et al., Reversible Compositional Control of Oxide Surfaces by Electrochemical Potentials. *J. Phys. Chem. Lett.* 3, 40-44 (2011). doi: 10.1021/jz201523y

[49] Z. Cai, M. Kubicek, J. Fleig et al., Chemical heterogeneities on La_{0.6}Sr_{0.4}CoO₃ δ thin films-correlations to cathode surface activity and stability. *Chem. Mater.* 24, 1116-1127 (2012). doi: 10.1021/cm203501u

[50] O. Celikbilek, G. Sassone, M. Prioux et al., Long-term tests and advanced post-test characterizations of the oxygen electrode in solid oxide electrolysis cells. *ECS Trans.* 111, 211 (2023). doi: 10.1149/11106.0211ecst

[51] Y. Chen, H. Téllez, M. Burriel et al., Segregated chemistry and structure on (001) surfaces of (La₁ Sr)₂CoO₄ override the crystal anisotropy in oxygen exchange kinetics. *Chem. Mater.* 27, 5436-5450 (2015). doi: 10.1021/acs.chemmater.5b02292

[52] X. Liu, L. Zhang, Y. Zheng et al., Uncovering the effect of lattice strain and oxygen deficiency on electrocatalytic activity of perovskite cobaltite thin films. *Adv. Sci.* 6, 1801898 (2019). doi: 10.1002/advs.201801898

[53] D. Oh, D. Gostovic, E.D. Wachsman. Mechanism of La_{0.6}Sr_{0.4}Co_{0.2}Fe_{0.8}O₃ cathode degradation. *J. Mater. Res.* 27, 1992-1999 (2012). doi: 10.1557/jmr.2012.222

[54] E.J. Crumlin, E. Mutoro, Z. Liu et al., Surface strontium enrichment on

highly active perovskites for oxygen electrocatalysis in solid oxide fuel cells. Energy Environ. Sci. 5, 6081–6088 (2012). doi: 10.1039/C2EE03397F

[55] E. Mutoro, E.J. Crumlin, H. Pöpke et al., Reversible Compositional Control of Oxide Surfaces by Electrochemical Potentials. J. Phys. Chem. Lett. 3, 40–44 (2012). doi: 10.1021/jz201523y

Note: Figure translations are in progress. See original paper for figures.

Source: ChinaXiv – Machine translation. Verify with original.